International Journal of Robotics and Control Systems
Vol. 5, No. 4, 2025, pp. 2325-2343
ISSN 2775-2658
http://pubs2.ascee.org/index.php/ijrcs

Comparative Analysis of Control Strategies for Tracking Periodic Sinusoidal References in Magnetic Levitation Systems

Attarid K. Ahmed [a,1], Huthaifa Al-Khazraji [a,2,*], Omar F. Lutfy [a,3], Ahmed S. Al-Araji [a,4]

[a] College of Artificial Intelligence Engineering, University of Technology-Iraq, Baghdad, 10066, Iraq
[1] Attarid.K.Ahmed@uotechnology.edu.iq; [2] 60141@uotechnology.edu.iq; [3] omar.f.lutfy@uotechnology.edu.iq;
[4] 60166@uotechnology.edu.iq
* Corresponding Author

ARTICLE INFO

Article history
Received August 04, 2025
Revised September 13, 2025
Accepted November 12, 2025

Keywords
Magnetic Levitation;
Nonlinear Control System;
Backstepping Control;
Synergetic Control;
Grasshopper Optimization Algorithm;
Trajectory Tracking

ABSTRACT

The dynamics associated with a magnetic levitation (Maglev) system are typically characterized by significant instability and nonlinear behavior. Consequently, the implementation of an effective control mechanism is imperative for achieving precise positioning of a ferromagnetic sphere. The majority of the extant literature primarily assesses the efficacy of the Maglev control system in response to a step input. This manuscript delineates a comparative analytical study contrasting synergetic control (SC) with backstepping control (BSC) in the context of a Maglev system aimed at tracking a periodic reference input. Periodic signals highlight how well the controller can achieve zero steady-state error (or minimal error) for non-constant references, which is harder than constant step tracking. The system's dynamics are articulated through the application of the Euler-Lagrange methodology. Utilizing the established nonlinear framework of the system, the control signals for both SC and BSC are formulated. Moreover, both control schemes were supplemented with the Grasshopper Optimization Algorithm (GOA), which was employed to systematically optimize the associated design parameters. The resultant optimized control systems are subjected to simulation utilizing MATLAB software. The findings from the simulations indicate that both proposed controllers effectively track the desired periodic reference input. Nevertheless, the quantitative analysis grounded in integral absolute error (IAE) metrics reveals that the performance of BSC surpasses that of SC.

1. Introduction

Magnetic levitation (Maglev) systems are widely used in industry because they operate without contact and friction, resulting in higher efficiency and lower mechanical wear, which in turn reduces maintenance costs [1]-[6]. In particular, the system features a ferromagnetic ball of specific mass that is suspended in an air gap by the magnetic force, which can be adjusted via the applied voltage [7]-[10]. However, owing to its nonlinear behavior and high instability, designing a control algorithm to keep the Maglev system stable is difficult. Consequently, numerous linear and nonlinear control methods have been developed to stabilize the system. For instance, Ahmad et al. [11] designed a Proportional-Integral-Derivative (PID) controller explicitly tailored for the Maglev system in response to a unit step input. To achieve optimal performance criteria, the tuning

parameters of the PID controller were meticulously optimized through the application of the Genetic Algorithm (GA). In comparison to the traditional Ziegler-Nichols (ZN) tuning approach, the simulation outcomes demonstrated that the efficacy of the PID controller significantly surpassed that achieved through the conventional ZN methodology. Furthermore, Benomair [12] introduces an optimal Linear Quadratic Regulator (LQR), optimized using an advanced spiral dynamic algorithm, for active regulation of a magnetic levitation system under full-state feedback linearization.

Simulation results based on the nonlinear Maglev model demonstrate the effectiveness of the proposed linearization and control scheme for both unit step and sinusoidal inputs. In a similar vein, Roy et al. [13] conducted a comparative analysis between the Fractional Order PID (FOPID) controller and the traditional PID controller to regulate the position of the ball within the Maglev system for step, sine-wave, and square-wave inputs. Three swarm optimization algorithms were utilized, specifically, the Gravitational Search Algorithm (GSA), the Particle Swarm Optimization (PSO), and a hybrid approach that merges these two techniques, known as PSOGSA. These algorithms were employed to optimize the parameters of the controllers. The findings from employing different test signals indicated that the PSOGSA hybrid algorithm outperformed the individual algorithms in terms of effectiveness. Additionally, the FOPID controller demonstrated greater effectiveness compared to the traditional PID controller. Furthermore, Ataşlar-Ayyildiz and Karahan [14] introduced a PID-like robust fuzzy logic controller (Fuzzy-PID) to improve the system dynamics and stability of the Maglev system under a pulse signal and a sinusoidal reference input. The Cuckoo Search (CS) algorithm was developed to optimize the parameters of the controller using time domain response characteristics as an objective function. Simulation experiments were carried out to assess the controller's performance across different conditions, such as load disturbances and reference adjustments. The findings showed that the CS-based Fuzzy-PID controller surpasses the conventional FOPID and PID controllers by achieving lower steady-state error, shorter settling time, and reduced overshoot, all while demanding less control effort.

In the development of a control mechanism for the nonlinear model of the Maglev system, Nguyen et al. [15] developed a feedback linearization-based state feedback controller (FL-SFC). In this approach, the nonlinear system was transformed into a linear system via feedback linearization, and then the state feedback controller method was used to address tracking control of the Maglev system. The BAT algorithm was proposed to optimize the design variables of the controller. The performance of the FL-SFC was further examined with the synergetic control (SC) by Al-Ani et al. [16]. The outcomes showed that the SC exhibited better control performance than that of the FL-SFC even when external disturbances were applied for a unit step input. The swarm bipolar algorithm (SBA) utilizes an error criterion for developing the cost function to find the best value of the gains of both controllers to achieve the desired response. Additionally, Chiem and Thang [17] proposed a linear feedforward control approach combined with a fuzzy logic controller (FLC) to regulate the Maglev system under step input conditions. Their design successfully preserved the ball's stability and improved the system's responsiveness to deviations from the equilibrium point. The control strategy was benchmarked against both a conventional PID controller and an independent FLC. Simulation results revealed that the method achieved a fast and stable response, even in the presence of noise. Nonetheless, a limitation of these studies is their reliance on the linear model of the Maglev system, and the examination was restricted to step input scenarios. In this context, sliding mode control has been employed by various researchers. For instance, Al-Muthairi and Zribi [18] introduced a sliding mode control (SMC) strategy designed to achieve the asymptotic regulation of the Maglev system's states to their designated step target values. To address the issue of chattering, two modifications to the original SMC were implemented. The resilience of the proposed control methodologies to variations in the system's parameters was thoroughly examined, revealing that these control methodologies exhibit robustness in the face of parameter fluctuations. Another utilization of the SMC methodology within the context of the Maglev system for step and sine-wave inputs was reported by Ma'arif et al. [19]. The system governed by the SMC exhibited a rapid output response devoid of any steady-state error. Nevertheless, the authors failed to address the issue of chattering within their investigation. In another study, Uswarman et al. [20] conducted a

comparative analysis between the Conventional Sliding Mode Control (CSMC) and the SMC incorporating gain-scheduling techniques to regulate the Maglev system to a step value target. The simulation results showed that the gain-scheduled SMC outperformed the CSMC when external disturbances were present. However, chattering remained an issue in both control methods. The challenge of chattering, as noted in [18], [19], and [20], persists as a limitation. To address this issue, the main contributions of this study are outlined as follows:

- Two distinct nonlinear control strategies, namely synergetic control (SC) and backstepping control (BSC), are proposed for stabilization and trajectory tracking of a periodic reference input of the Maglev system, employing the nonlinear model of the system across a variety of operational conditions.
- The proposed control strategies' stability is analyzed using Lyapunov stability theory.
- The grasshopper optimization algorithm is employed as a means to optimally calibrate the tuning parameters of the proposed controllers, to improve the system's dynamic performance.

2. The Mathematical Model

The magnetic levitation (Maglev) system is comprised of a ferromagnetic sphere elevated within a voltage-regulated magnetic field [21]. The primary aim of the Maglev control system is to attain exceptional precision in the localization of the diminutive steel sphere in a fixed position under conditions of stable levitation [22]. A schematic representation of the Maglev system is depicted in Fig. 1 [16], [19]. In particular, the parameters of the system, along with their corresponding symbols, include the electromagnetic force (fe), the gravitational force (fg), the inductance (L), the resistance (R), the position of the object (x), the source voltage (V), the mass of the object (m), and the current. The dynamics governing the mechanical components of the Maglev system can be articulated by Newton's second law of motion, as delineated [10]:

$$m\frac{d^2x}{dt^2} = fg - fe \tag{1}$$

which are represented as follows for the electromagnetic and gravitational forces:

$$fg = mg \tag{2}$$

$$fe = \frac{1}{2}i^2\frac{d}{dx}\left(L(x)\right) \tag{3}$$

The function Lx is a nonlinear function that can be written as follows:

$$L(x) = L + L_0x_0 \tag{4}$$

Equation (4) can be approximated as [17]:

$$L(x) = \frac{2k}{x^2} \tag{5}$$

where k is the force constant. Substituting Eq. (5) in Eq. (3) gives:

$$fe = k\left(\frac{i}{x}\right)^2 \tag{6}$$

Substituting Eqs. (2) and (6) in Eq. (1) give:

$$m\frac{d^2x}{dt^2} = mg - k\left(\frac{i}{x}\right)^2 \tag{7}$$

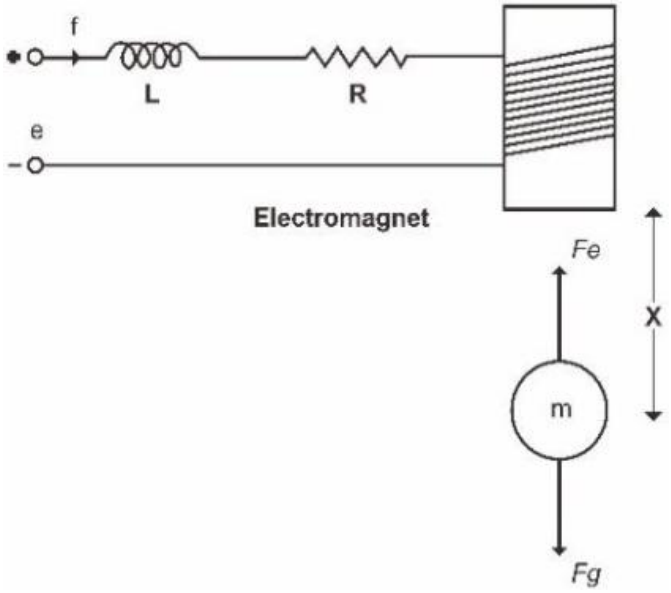

Fig. 1. The Maglev system

By rearranging Eq. (7), we get:

$$\frac{d^2x}{dt^2} = g - \frac{k}{m}\left(\frac{i}{x}\right)^2 \tag{8}$$

In addition to the mechanical analysis, Kirchhoff's voltage law applied to the electrical system is employed to obtain Eq. (9).

$$e = iR + \frac{d}{dt} L(x)i \tag{9}$$

Through straightforward mathematical manipulation, the equation can be expressed as:

$$\frac{di}{dt} = -\frac{R}{Li} - \frac{2k}{L}\frac{i}{x^2}\frac{dx}{dt} + \frac{1}{L}e \tag{10}$$

Given that the system states are: $x_1 = x, x_2 = \frac{dx}{dt}$ and $x_3 = I$, the control input is $u = e$, the nonlinear differential equations that describe the dynamics of the Maglev system are shown.

$$\frac{dx_1}{dt} = x_2 \tag{11}$$

$$\frac{dx_2}{dt} = g - \frac{kx_3^2}{mx_1^2} \tag{12}$$

$$\frac{dx_3}{dt} = -\frac{Rx_3}{L} + \frac{2kx_2x_3}{Lx_1^2} + \frac{u}{L} \tag{13}$$

where $x_1 > 0$ and $x_3 > 0$.

The system's output y can be described as:

$$y = x_1 \tag{14}$$

Nonlinearity attributes are evident in Equations (12) and (13), as demonstrated by the Maglev system's operation. To aid controller design, the Maglev model is transformed into an equivalent

canonical form, offering a simpler representation that highlights nonlinearity via a single dynamic equation. Specifically, this nonlinear coordinate transformation is described as:

$$z_1 = x_1 \tag{15}$$

$$z_2 = x_2 \tag{16}$$

$$z_3 = g - \frac{kx_3^2}{mx_1^2} \tag{17}$$

Therefore, the model in the new coordinate system can be represented as:

$$\dot{z}_1 = z_2 \tag{18}$$

$$\dot{z}_2 = z_3 \tag{19}$$

$$\dot{z}_3 = f(z) + g(z)\, u \tag{20}$$

Where

$$f(z) = \frac{2kR\, x_3^2}{mx_1^2 L} - \frac{4k^2\, x_3^2 x_2}{mx_1^4 L} + \frac{2kx_2 x_3^2}{mx_1^3} \tag{21}$$

$$g(z) = -\frac{2kx_3}{mx_1^2 L} \tag{22}$$

3. Controller Design

The application of feedback controllers is perpetually broadening to encompass a diverse array of systems [23]-[26]. Within this framework, the regulation of the Maglev system necessitates addressing various challenges, including tracking control and managing external disturbances. In this regard, this particular section delves into two nonlinear control methodologies aimed at formulating the control law for the Maglev system, namely the synergetic control (SC) and the backstepping control (BSC). These two nonlinear controllers are particularly advantageous for the Maglev system, as they proficiently address the system's nonlinear dynamics, thereby facilitating prompt and stable positioning of the levitated object while concurrently preserving robustness against disturbances.

3.1. Synergetic Control

SC constitutes a methodological approach applicable to a diverse array of dynamical systems, with particular efficacy in the context of nonlinear dynamical systems, in order to achieve a stable control paradigm [27], [28]. More precisely, the methodology for the formulation of SC is delineated as follows:

Quantify e as the discrepancy between the actual outputs and the desired outputs.

$$e = z_r - z_1 \tag{23}$$

Taking the derivative of the error gives:

$$\dot{e} = \dot{z}_r - \dot{z}_1 \tag{24}$$

By substituting Eq. (18) in Eq. (24), we get:

$$\dot{e} = \dot{z}_r - z_2 \tag{25}$$

Taking the second derivative of the error gives:

$$\ddot{e} = \ddot{z}_r - \dot{z}_2 \tag{26}$$

Substituting Eq. (19) in Eq. (26) gives:

$$\ddot{e} = \ddot{z}_r - z_3 \tag{27}$$

By taking the third derivative of the error, we get:

$$\dddot{e} = \dddot{z}_r - \dot{z}_3 \tag{28}$$

Substituting Eq. (20) in Eq. (28) gives:

$$\dddot{e} = \dddot{z}_r - f(z) - g(z)\, u \tag{29}$$

Define a macro-variable σ as:

$$\sigma = c_1 e + c_2 \dot{e} + \ddot{e} \tag{30}$$

Taking the derivative of the macro-variable σ gives:

$$\dot{\sigma} = c_1 \dot{e} + c_2 \ddot{e} + \dddot{e} \tag{31}$$

The desired dynamic evolution of the macro-variable is:

$$\dot{\sigma} + c_3\, \sigma = 0 \tag{32}$$

$$\dot{\sigma} = -c_3\, \sigma \tag{33}$$

Substituting Eq. (31) in Eq. (32) gives:

$$c_1 \dot{e} + c_2 \ddot{e} + \dddot{e} + c_3\, \sigma = 0 \tag{34}$$

By substituting $\dddot{e}$ given by Eq. (29) in Eq. (34), we obtain:

$$c_1 \dot{e} + c_2 \ddot{e} + \dddot{z}_r - f(z) - g(z)\, u + c_3\, \sigma = 0 \tag{35}$$

Select u as follows:

$$u_{sc} = \frac{1}{g(z)} \left(-f(z) + \dddot{z}_r + c_1 \dot{e} + c_2 \ddot{e} + c_3\, \sigma\right) \tag{36}$$

Choose the Lyapunov function as:

$$V = \frac{1}{2} \sigma^2 \tag{37}$$

Taking the derivative of V gives:

$$\dot{V} = \sigma\, \dot{\sigma} \tag{38}$$

Substitute Eq. (33) in Eq. (38):

$$\dot{V} = \sigma\, (-c_3\, \sigma\,) \tag{39}$$

$$\dot{V} = -c_3\, \sigma^2 \tag{40}$$

Equation (40) ensures the stability of the closed-loop system given based on the SC approach.

3.2. Backstepping Control

BSC represents a sophisticated control methodology that can be implemented across diverse dynamical systems, particularly within the realm of nonlinear dynamical systems, to achieve a stable control paradigm. In summary, the BSC constitutes a recursive and systematic approach to control that utilizes the Lyapunov function as a foundational tool for formulating the control law [29]. More specifically, in the design of the BSC, we define the error, e_1, as the discrepancy between the actual outputs and the desired outputs:

$$e_1 = z_r - z_1 \tag{41}$$

Taking the derivative of the error gives:

$$\dot{e}_1 = \dot{z}_r - z_2 \tag{42}$$

Additionally, z_2 is chosen as the virtual control v_1 and substituted into Eq. (42) to obtain:

$$\dot{e}_1 = \dot{z}_r - v_1 \tag{43}$$

The first Lyapunov function is selected as:

$$V_1 = \frac{1}{2}{e_1}^2 \tag{44}$$

Taking the time derivative of V_1 obtians:

$$\dot{V}_1 = e_1\dot{e}_1 = e_1(\dot{z}_r - v_1) \tag{45}$$

Selecting virtual control v as:

$$v_1 = \dot{z}_r + \lambda_1 e_1 \tag{46}$$

where $\lambda_1 > 0$,

By substituting v_1 obtained in Eq. (46) into Eq. (45) yields:

$$\dot{V}_1 = -\lambda_1{e_1}^2 \tag{47}$$

Define the error e_2 between the virtual control v_1 and z_2 as:

$$e_2 = z_2 - v_1 \tag{48}$$

Substituting v_1 given by Eq. (46) in Eq. (48) gives:

$$e_2 = z_2 - \dot{z}_r - \lambda_1 e_1 \tag{49}$$

Solving Eq. (49) for z_2, and then, substituting z_2 in Eq. (43) give:

$$\dot{e}_1 = -e_2 - \lambda_1 e_1 \tag{50}$$

Taking the time derivative of e_2 obtains:

$$\dot{e}_2 = z_3 - \ddot{z}_r - \lambda_1\dot{e}_1 \tag{51}$$

z_3 is selected as the virtual control v_2.

By using v_2 in Eq. (51) gives:

$$\dot{e}_2 = v_2 - \ddot{z}_r - \lambda_1\dot{e}_1 \tag{52}$$

The second Lyapunov function is selected as:

$$V_2 = \frac{1}{2}{e_1}^2 + \frac{1}{2}{e_2}^2 \tag{53}$$

Taking the time derivative of V_2 gives:

$$\dot{V}_2 = e_1\dot{e}_1 + e_2\dot{e}_2 \tag{54}$$

Substituting Eq. (40) and Eq. (52) in Eq. (54) gives:

$$\dot{V}_2 = e_1(-e_2 - \lambda_1 e_1) + e_2(v_2 - \ddot{z}_r - \lambda_1\dot{e}_1) \tag{55}$$

Rearranging Eq. (55) gives:

$$\dot{V}_2 = -\lambda_1{e_1}^2 + e_2(-e_1 + v_2 - \ddot{z}_r - \lambda_1\dot{e}_1) \tag{56}$$

The virtual control v_2 is selected as:

$$v_2 = -\lambda_2 e_2 + \lambda_1\dot{e}_1 + e_1 + \ddot{z}_r \tag{57}$$

where $\lambda_2 > 0$

Substituting v_2 in Eq. (56) gives:

$$\dot{V}_2 = -\lambda_1{e_1}^2 - \lambda_2{e_2}^2 \tag{58}$$

Define e_3 as the error between the virtual control v_2 and z_3:

$$e_3 = z_3 - v_2 \tag{59}$$

Substituting v_2 in Eq. (57) gives:

$$e_3 = z_3 + \lambda_2 e_2 - \lambda_1\dot{e}_1 - e_1 - \ddot{z}_r \tag{60}$$

Solving Eq. (60) for z_3, and then substituting z_3 in Eq. (51) give:

$$\dot{e}_2 = -\lambda_2 e_2 + e_3 + e_1 \tag{61}$$

By taking the derivative of e_3 and substituting $\dot{z}_3$ as given in Eq. (20), we attain:

$$\dot{e}_3 = f(z) + g(z)u + \lambda_2\dot{e}_2 + \lambda_1\dot{e}_2 + \lambda_1^2\dot{e}_1 - \dot{e}_1 - \dddot{z}_r \tag{62}$$

Choosing the first Lyapunov function and taking the derivative gives:

$$V_3 = \frac{1}{2}{e_1}^2 + \frac{1}{2}{e_2}^2 + \frac{1}{2}{e_3}^2 \tag{63}$$

$$\dot{V}_3 = e_1\dot{e}_1 + e_2\dot{e}_2 + e_3\dot{e}_3 \tag{64}$$

Substituting $\dot{e}_1$, $\dot{e}_2$, and $\dot{e}_3$ gives:

$$\dot{V}_3 = e_1(-e_2 - \lambda_1 e_1) + e_2(-\lambda_2 e_2 + e_3 + e_1) + e_3(f(x) + g(x)u + \lambda_2\dot{e}_2 + \lambda_1\dot{e}_2 + \lambda_1^2\dot{e}_1 - \dot{e}_1 - \dddot{z}_r) \tag{65}$$

Rearranging Eq. (65) gives:

$$\dot{V}_3 = -\lambda_1{e_1}^2 - \lambda_2{e_2}^2 + e_3(f(x) + g(x)u + \lambda_2\dot{e}_2 + \lambda_1\dot{e}_2 + \lambda_1^2\dot{e}_1 - \dot{e}_1 - \dddot{z}_r) \tag{66}$$

Then, u is selected as follows:

$$u_{bsc} = \frac{1}{g(x)}(-f(x) - \lambda_2\dot{e}_2 - \lambda_1\dot{e}_2 - \lambda_1^2\dot{e}_1 - e_2 + \dot{e}_1 - \dddot{z}_r - \lambda_3 e_3) \tag{67}$$

where $\lambda_3 > 0$

Substituting u in Eq. (66) gives;

$$\dot{V}_3 = -\lambda_1 {e_1}^2 - \lambda_2 {e_2}^2 - \lambda_3 {e_3}^2 \tag{68}$$

Equation (68) ensures the stability of the closed-loop system based on the BSC approach.

4. The Grasshopper Optimization Algorithm

The swarm optimization algorithm employs an iterative and stochastic methodology for addressing a variety of complex problems [30]-[36]. To this end, a plethora of swarm optimization algorithms exists within the academic literature, specifically designed to enhance the design parameters of diverse control systems [37]-[46]. This manuscript elucidates the Grasshopper Optimization Algorithm (GOA), which represents a contemporary approach to swarm optimization used for calibrating design variables of the proposed controllers implemented for the Maglev system. Saremi et al. [47] have elucidated the concept of GOA, which delineates the behavioral characteristics of grasshoppers. In this regard, the grasshoppers are recognized for their detrimental effects on agricultural production and crop yields. These insects exhibit gregarious behavior, traveling in swarms and consuming the flora encountered in their path. The size of the grasshopper swarm is considerable, instilling a sense of trepidation in farmers regarding potential devastation.

When in the nymphal stage, grasshoppers exhibit the absence of wings and display a lethargic locomotion, aligning themselves with the prevailing wind in a manner reminiscent of rolling cylinders. Upon reaching adulthood, they congregate in substantial swarms, engaging in aerial flight that enables them to traverse considerable distances [48]. The intrinsic characteristics of grasshoppers motivated researchers to delineate the process into two distinct phases: exploration and exploitation, in conjunction with the pursuit of specific targets. However, there exists a notable differentiation in the modes of movement associated with these two operational functions. Particularly, the agents exhibit stochastic behavior during the exploration phase, while they demonstrate localized movement during the exploitation phase. The migratory dynamics of the grasshoppers can be quantitatively represented as follows [49]:

$$Z_i = \Psi_i + \Gamma_i + \Omega_i \tag{69}$$

where Z_i denotes the position of the i-th grasshopper, Ψ_i represents the social interactions among individuals, Γ_i is indicative of the gravitational force, and Ω_i denotes the influence of wind advection. This mathematical formulation can elucidate the stochastic behavior of grasshoppers by incorporating a random variable r, constrained within the range [0,1], as demonstrated:

$$Z_i = r\Psi_i + r\Gamma_i + r\Omega_i \tag{70}$$

Social interaction Ψi can be influenced by other parameters, as illustrated in the equations (71) [50]:

$$\Psi_i = \sum_{\substack{j=1 \\ j \neq i}}^{N} \psi(d_{ij}) \widehat{d_{ij}} \tag{71}$$

$$\psi(r) = fe^{-r/l} - e^{-r} \tag{72}$$

$$d_{ij} = |z_j - z_i| \tag{73}$$

$$\widehat{d_{ij}} = \frac{z_j - z_i}{d_{ij}} \tag{74}$$

It is clear that the equation governing social interaction involves variables ψ representing the strength of social forces, as explained in Equation (72). In Equation (72), the variable f indicates the level of attraction, l represents the attractive length scale, and dij denotes the distance between the i-th and the j-th grasshoppers, as shown in Equation (73). Furthermore, Equation (74) describes the unit vector dij that points from the i-th to the j-th grasshopper.

It has been empirically established that the function ψ exerts a significant influence on social interactions f and l, such that any modification therein results in repercussions regarding the magnitude of the social force. Consequently, this influences social interactions, attraction, repulsion, and the grasshoppers' comfort zones. The space between any two grasshoppers is classified into repulsion, attraction, and comfort zones. If the distance is large, it is divided into smaller segments. The gravity force Γi can be calculated as shown in Equation (75):

$$\Gamma i = -g\widehat{e_g} \tag{75}$$

where g is the gravitational constant, and $\widehat{e_g}$ is the unit vector directed towards the center of the Earth. The final term in the positional Equation (69) represents the phenomenon of wind advection, which can be expressed as follows:

$$\Omega_i = \rho\widehat{e_w} \tag{76}$$

where ρ is a constant, and $\widehat{e_w}$ is a unity vector in the wind direction. Substituting Ψ_i, Γ_i , and Ω_i in Eq. (69) gives:

$$Z_i = \sum_{\substack{j=1 \\ j\neq i}}^{N} \psi\left(\left|z_j - z_i\right|\right)\frac{z_j - z_i}{d_{ij}} - g\widehat{e_g} + \rho\widehat{e_w} \tag{77}$$

Through the application of Equation (77), it has been demonstrated that the grasshoppers attain their optimal comfort zone and refrain from departing from it. This phenomenon has resulted in a diminishment of efficacy in the processes of exploration and exploitation in the resolution of the problem. Consequently, it is evident that this mathematical framework is not suitable for addressing the optimization issue; thus, a revised iteration of this equation has been proposed, as delineated in Eq. (78), [51]:

$$Z_i^d = \eta\left(\sum_{\substack{j=1 \\ j\neq i}}^{N} \eta\frac{ub_d - lb_d}{2}\,\psi\left(\left|z_j^d - z_i^d\right|\right)\frac{z_j - z_i}{d_{ij}}\right) + \widehat{T_d} \tag{78}$$

In this context, Ψ_i is nearly identical, Γi is ignored, and Ω_i is assumed to point toward the target $\widehat{T_d}$. The terms ub_d and lb_d represent the upper and the lower bounds in the D-th dimension. $\widehat{T_d}$ corresponds to the value in that dimension, and η is a coefficient that reduces the size of the comfort, repulsion, and attraction zones. Td indicates how likely the grasshopper is to move toward the target. The remainder of Eq. (78) describes how grasshoppers interact, taking into account their peers' positions.

In Equation (78), the initial term delineates the spatial positioning of the extant grasshopper relative to the other grasshoppers within the framework. This particular algorithm exhibits distinctive characteristics that set it apart from alternative optimization methodologies. In the process of updating the positions of grasshoppers within the GOA, the current position, the target position, and the positions of all other grasshoppers are employed. Furthermore, it is noteworthy that the GOA utilizes a singular vector for each search agent, in contrast to other optimization algorithms, which typically utilize dual vectors to represent velocity and position.

It is observable that Equation (78) contains two instances of the variable η, each serving a distinct function. The initial instance of η, positioned on the left, operates as the inertial weight analogous to that used in Particle Swarm Optimization (PSO). It is tasked with regulating the dynamics of grasshopper movement in the contexts of exploration and exploitation surrounding the targeted area as the iterations progress. Conversely, the internal mechanisms function to diminish the zones of repulsion, attraction, and comfort among grasshoppers, coinciding with a reduction in the number of iterations. In particular, the GOA initiates the exploratory phase to ascertain appropriate search domains. Subsequently, the exploitation phase guides the agent to conduct a localized search for the global optimum, which is contrary to the inherent movement patterns of grasshoppers. Consequently, the parameter η is employed to mediate the interplay between exploration and exploitation, as indicated in Equation (79), [52]:

$$\eta = \eta_{max} - k\frac{\eta_{max} - \eta_{min}}{K} \tag{79}$$

where η_{max} is the apex value, which is established at 1, η_{min} is the nadir value, which is established at 0.00001, k denotes the current iteration, and K signifies the upper limit of iterations. In pursuit of the global optimal solution within the framework of the GOA, the grasshoppers navigate towards the individual exhibiting the most favorable value during each iteration. This methodology is anticipated to yield the most accurate approximation of the optimal real solution within the defined search space.

5. Simulation Results

The Maglev system with BSC and SC was simulated using the MATLAB simulation platform. The physical parameters of the elements within the Maglev system are presented in Table 1 [15]. The initial conditions of the system were set with a position of 1 mm, a velocity of zero, and a current of 0.3A. To optimize the performance of both the BSC and the SC, the GOA is employed to fine-tune the design parameters of each controller. Additionally, the performances of the BSC and the SC are enhanced by adjusting the parameters ($c_1, c_2,$ and c_3) and ($\lambda_1, \lambda_2,$ and λ_3) of the control laws specified in Eq. (36) and Eq. (67), respectively.

Table 1. Parameters of the Maglev system

Parameters	Values
Resistance (R)	11.4 Ω
Inductance (L)	0.6 H
Mass (m)	0.006 Kg
Gravity acceleration (g)	9.81 m/s2
Force constant (k)	1.4×10-4 Nm2/A2

The cost function based on the Summation of Absolute Errors (SAE), as shown in Eq. (80), is used to guide the optimization process toward the best performance [53]-[55].

$$\text{Cost Function}_{SAE} = \sum_{i=1}^{T_f} |e(i)| \tag{80}$$

where T_f refers to the total number of samples in the simulation. The design variables of the BSC and the SC are reported in Table 2.

5.1. Evaluation in Normal Conditions

Fig. 2 illustrates the responses of the Maglev system to the periodic sinusoidal input. The tracking error associated with the system employing the BSC and the SC is depicted in Fig. 3.

Moreover, the resultant control signals produced by the proposed controllers are represented in Fig. 4. In this regard, a comparative analysis of the two control methodologies (BSC and SC), as presented in Fig. 2 and Fig. 3, reveals that the Maglev system utilizing both controllers is proficiently tracking the intended reference input. Nonetheless, the quantitative findings enumerated in Table 3 pertaining to the SAE indicate that the BSC exhibits a superior tracking response to the desired reference in comparison to the SC, with the SAE diminishing from 4.1 mm for the SC to 3.7 mm for the BSC. Consequently, the BSC realizes a 9.7% enhancement in SAE relative to the SC, thereby underscoring its superior tracking capability under standard operational conditions.

Table 2. Optimal setting of the controllers

Controller	Parameter	Value
BSC	c_1	125
	c_2	20
	c_3	75
SC	λ_1	80
	λ_2	50
	λ_3	12

5.2. Evaluation Under External Disturbances

Fig. 5 illustrates how the Maglev system reacts to a periodic sine-wave input when subjected to external disturbances. Fig. 6 displays the tracking error of the system utilizing both the BSC and the SC methods. In addition, the control signals produced by the proposed controllers are depicted in Fig. 7. By examining Fig. 5 and Fig. 6, it is evident that the Maglev system, when employing both controllers, effectively tracks the desired reference input even in the presence of external disturbances. However, the data presented in Table 4 for the SAE indicate that the BSC offers a more effective tracking response to the desired reference when faced with external disturbances compared to the SC. Specifically, the SAE decreases from 10.6mm with the SC to 6.2mm with the BSC. Consequently, the BSC demonstrates a 41.5% enhancement in SAE over the SC, highlighting its superior tracking performance under external disturbances.

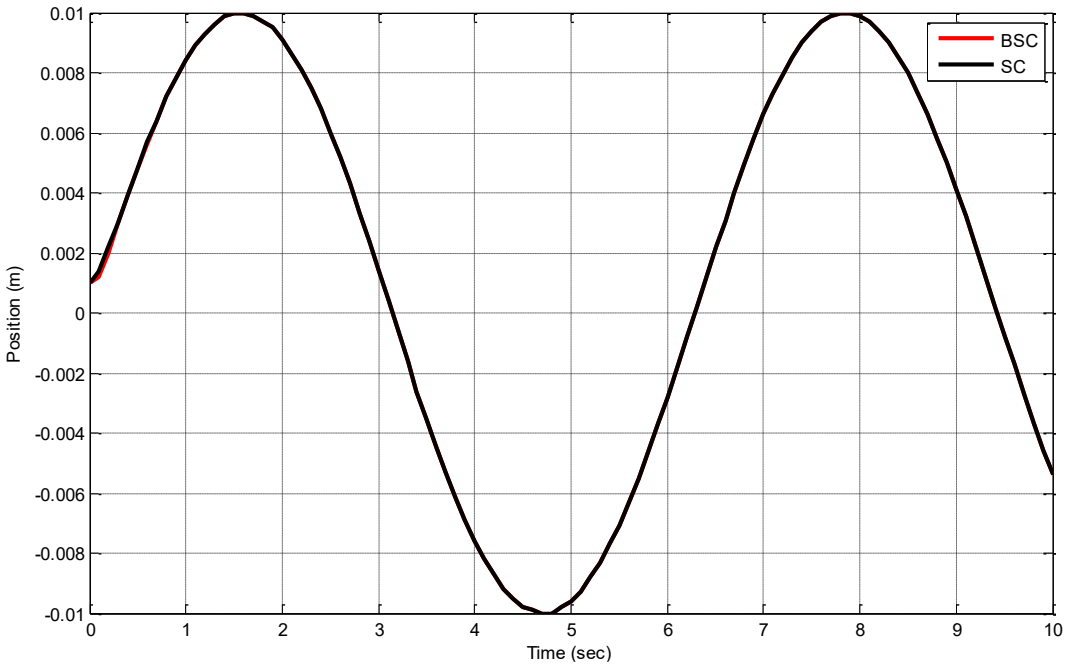

Fig. 2. Response of tracking position of Maglev based on BSC and SC under normal conditions

The aforementioned simulation results demonstrate that the BSC is capable of effectively controlling the Maglev system in a better manner compared to the SC for the two studied scenarios. These scenarios encompass both normal operation and the impact of external disturbances.

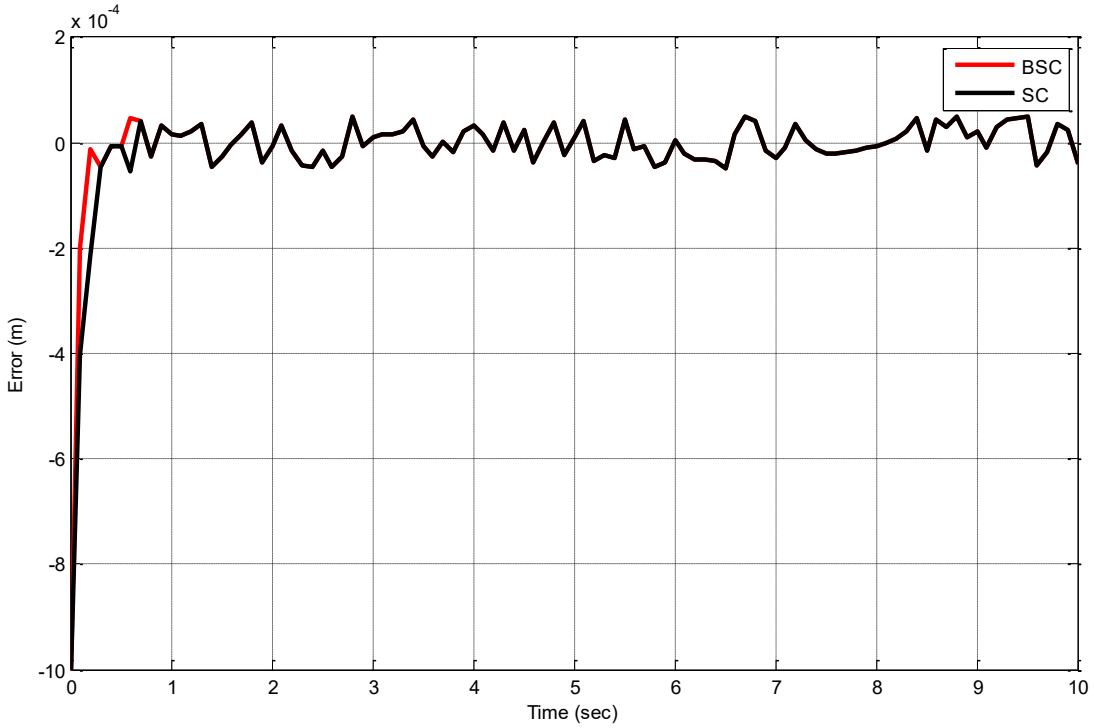

Fig. 3. Response of tracking error of Maglev based on BSC and SC under normal operation

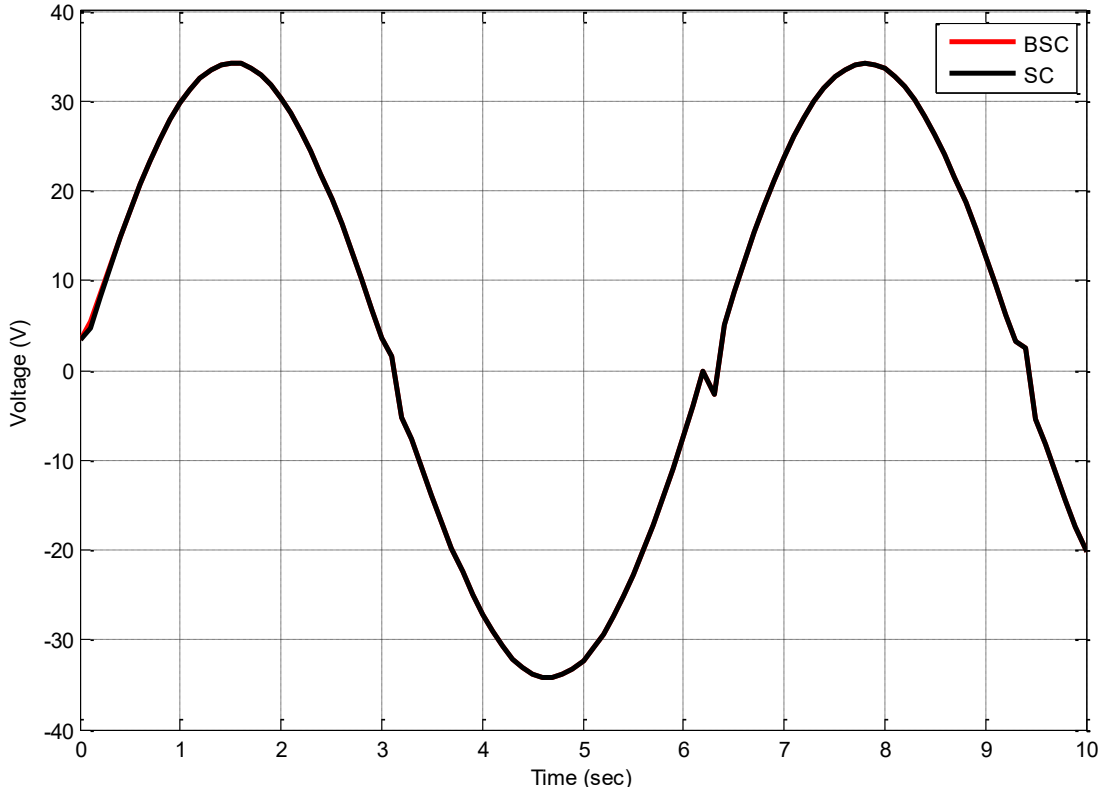

Fig. 4. Control signals of BSC and SC under normal operation

Table 3. SAE index under normal operation

Controller	SAE (mm)
BSC	3.7
SC	4.1

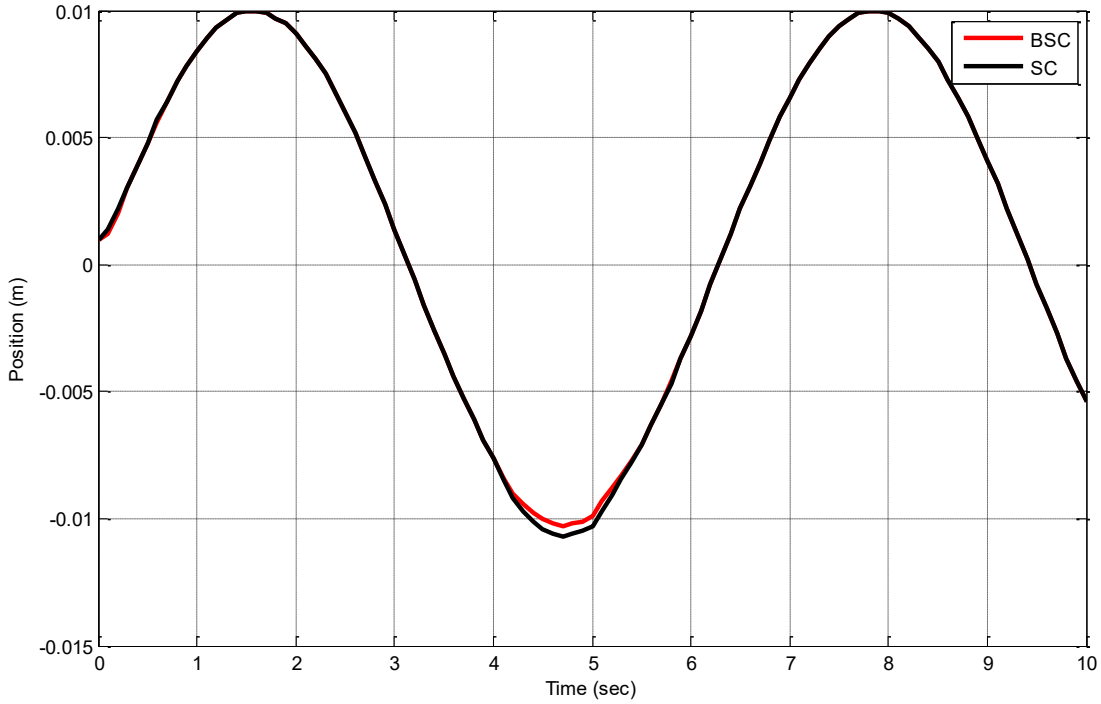

Fig. 5. Response of tracking position of Maglev based on BSC and SC under external disturbance

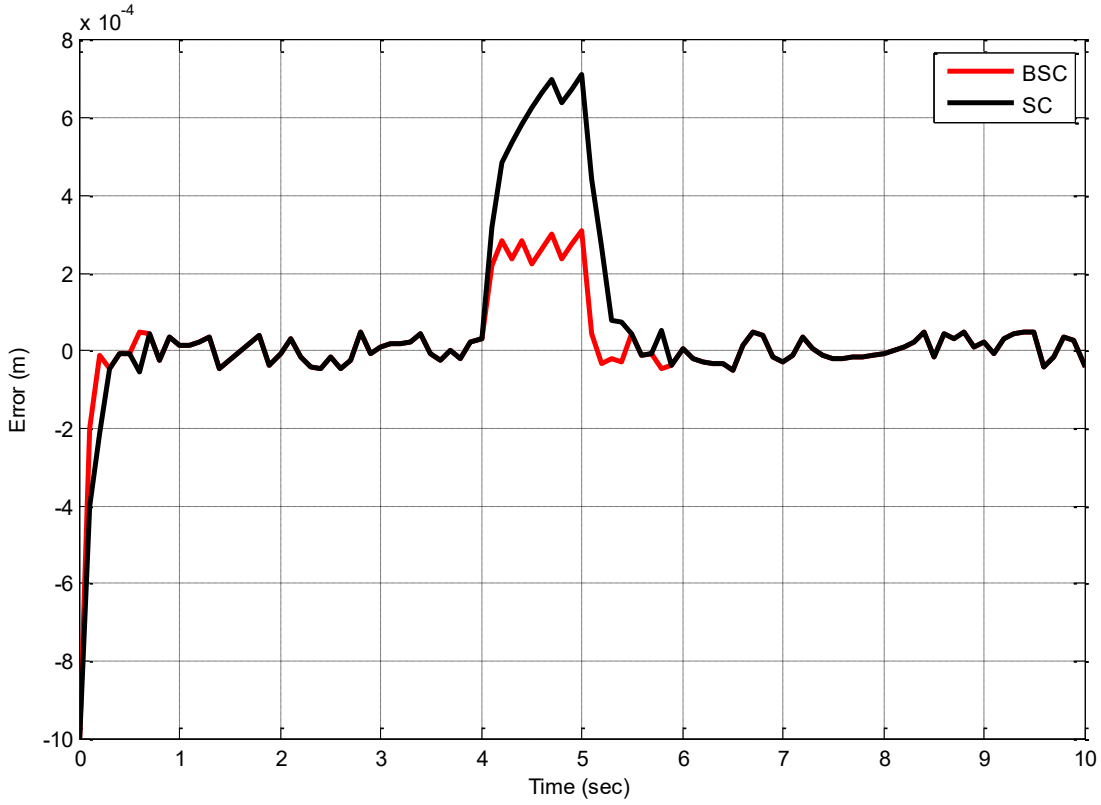

Fig. 6. Response of tracking error of Maglev based on BSC and SC under external disturbance

Table 4. SAE under external disturbance

Controller	SAE (mm)
BSC	6.2
SC	10.6

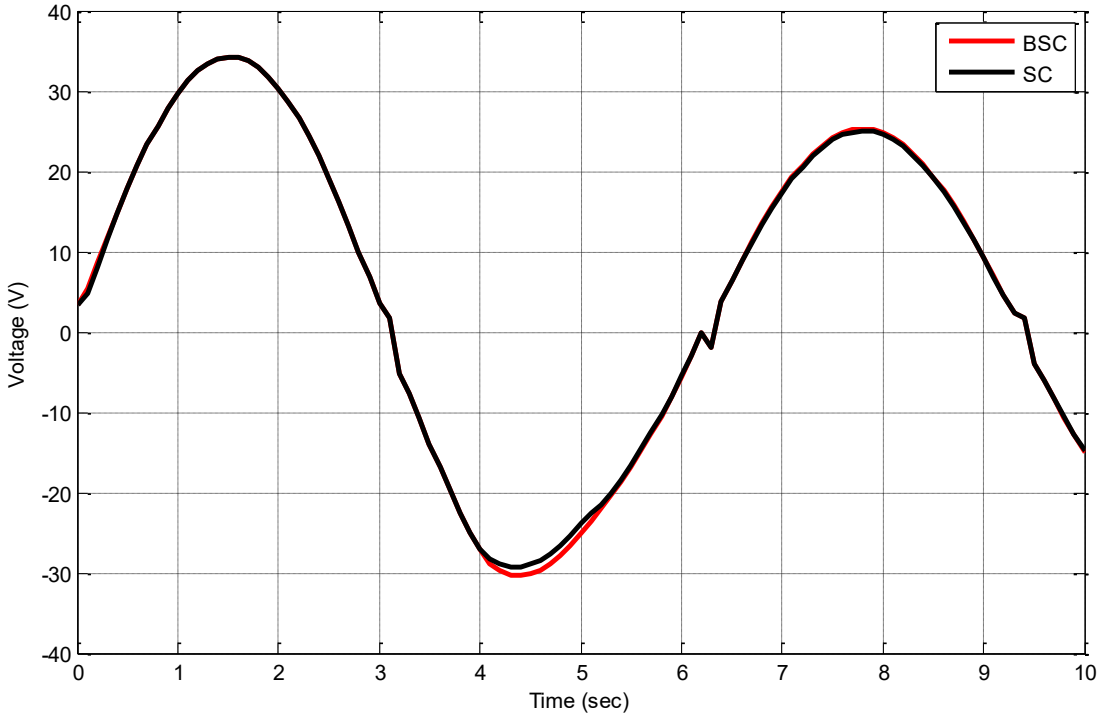

Fig. 7. Control signals of BSC and SC under external disturbance

6. Conclusion

This study investigated the design and enhancement of synergetic control (SC) and backstepping control (BSC) for a Maglev system, focusing on tracking periodic sinusoidal reference inputs. The GOA was employed to address the challenges associated with manually tuning the design parameters of each controller. To validate the effectiveness of the developed controllers, a comparative computer simulation was performed using MATLAB. The simulation outcomes indicate that the BSC offers superior dynamic tracking performance and robustness compared to the SC, both under normal conditions and in the presence of disturbances. Specifically, under normal operation, the BSC achieved a 9.7% improvement in the SAE over the SC, highlighting its enhanced tracking capability. Conversely, when the Maglev system encountered a disturbance, the BSC demonstrated a 41.5% improvement in SAE over the SC, underscoring its superior tracking performance under external disturbances. As a result, the improved tracking response and disturbance rejection for periodic reference inputs make the BSC particularly suitable for applications that require quick stabilization. Future research could focus on assessing the BSC's performance in more complex scenarios, including non-linear disturbances and parameter variations, as well as testing its implementation on physical hardware for practical validation.

Author Contribution: All authors contributed equally to the main contributor to this paper. All authors read and approved the final paper.

Funding: This research received no external funding.

Conflicts of Interest: The authors declare no conflict of interest.

References

[1] A. Bizuneh, H. Mitiku, A. O. Salau and K. Chandran, "Performance analysis of an optimized PID-P controller for the position control of a magnetic levitation system using recent optimization algorithms," *Measurement: Sensors*, vol. 33, p. 101228, 2024, https://doi.org/10.1016/j.measen.2024.101228.

[2] K. Hu, H. Jiang, Q. Zhu, W. Qian, and J. Yang, "Magnetic levitation belt conveyor control system based on multi-sensor fusion," *Applied Sciences*, vol. 13, no. 13, p. 7513, 2023, https://doi.org/10.3390/app13137513.

[3] P. Kumar, M. Ansari, E. Toyserkani, and M. B. Khamesee, "Experimental implementation of a magnetic levitation system for laser-directed energy deposition via powder feeding additive manufacturing applications," *Actuators*, vol. 12, no. 6, p. 244, 2023, https://doi.org/10.3390/act12060244.

[4] S. Ge, A. Nemiroski, K. A. Mirica, C. R. Mace, J. W. Hennek, A. A. Kumar, and G. M. Whitesides, "Magnetic levitation in chemistry, materials science, and biochemistry," *Angewandte Chemie International Edition*, vol. 59, no. 41, pp. 17810-17855, 2020, https://doi.org/10.1002/anie.201903391.

[5] R. S. Gopi, S. Srinivasan, K. Panneerselvam, Y. Teekaraman, R. Kuppusamy, and S. Urooj, "Enhanced model reference adaptive control scheme for tracking control of magnetic levitation system," *Energies*, vol. 14, no. 5, p. 1455, 2021, https://doi.org/10.3390/en14051455.

[6] E. V. Kumar and J. Jerome, "LQR based optimal tuning of PID controller for trajectory tracking of magnetic levitation system," *Procedia Engineering*, vol. 64, pp. 254-264, 2013, https://doi.org/10.1016/j.proeng.2013.09.097.

[7] P. Majewski, D. Pawuś, K. Szurpicki and W. P. Hunek, "Toward optimal control of a multivariable magnetic levitation system," *Applied Sciences*, vol. 12, no. 2, p. 674, 2022, https://doi.org/10.3390/app12020674.

[8] W. Bauer and J. Baranowski, "Fractional PI λ D controller design for a magnetic levitation system," *Electronics*, vol. 9, no. 12, p. 2135, 2020, https://doi.org/10.3390/electronics9122135.

[9] S. Dey, J. Dey and S. Banerjee, "Optimization Algorithm Based PID Controller Design for a Magnetic Levitation System," *2020 IEEE Calcutta Conference (CALCON)*, pp. 258-262, 2020, https://doi.org/10.1109/CALCON49167.2020.9106522.

[10] A. Abbas *et al*., "Design and Control of Magnetic Levitation System," *2019 International Conference on Electrical, Communication, and Computer Engineering (ICECCE)*, pp. 1-5, 2019, https://doi.org/10.1109/ICECCE47252.2019.8940711.

[11] I. Ahmad, M. Shahzad and P. Palensky, "Optimal PID control of Magnetic Levitation System using Genetic Algorithm," *2014 IEEE International Energy Conference (ENERGYCON)*, pp. 1429-1433, 2014, https://doi.org/10.1109/ENERGYCON.2014.6850610.

[12] A. M. Benomair, F. A. Bashir and M. O. Tokhi, "Optimal control based LQR-feedback linearisation for magnetic levitation using improved spiral dynamic algorithm," *2015 20th International Conference on Methods and Models in Automation and Robotics (MMAR)*, pp. 558-562, 2015, https://doi.org/10.1109/MMAR.2015.7283936.

[13] P. Roy, M. Borah, L. Majhi and N. Singh, "Design and implementation of FOPID controllers by PSO, GSA and PSOGSA for MagLev system," *2015 International Symposium on Advanced Computing and Communication (ISACC)*, pp. 10-15, 2015, https://doi.org/10.1109/ISACC.2015.7377307.

[14] B. Ataşlar-Ayyildiz and O. Karahan, "Trajectory Tracking for the Magnetic Ball Levitation System via Fuzzy PID Control Based on CS Algorithm," *2019 IEEE International Symposium on INnovations in Intelligent SysTems and Applications (INISTA)*, pp. 1-6, 2019, https://doi.org/10.1109/INISTA.2019.8778271.

[15] X. C. Nguyen, D. L. Hoang, X. T. Pham, T. H. Nguyen, M. K. Le, and V. X. Nguyen, "Synthesis of feedback linearization controller with parameters optimization based on bat algorithm for a magnetic levitation system," *Journal of Science and Technique*, vol. 16, no. 03, pp. 123-139, 2021, https://doi.org/10.56651/lqdtu.jst.v16.n03.283.

[16] F. R. Al-Ani, O. F. Lutfy, and H. Al-Khazraji, "Optimal Synergetic and Feedback Linearization Controllers Design for Magnetic Levitation Systems: A Comparative Study," *Journal of Robotics and Control*, vol. 6, no. 1, pp. 22-30, 2024, https://doi.org/10.18196/jrc.v6i1.24452.

[17] N. X. Chiem and L. T. Thang, "Synthesis of Hybrid Fuzzy Logic Law for Stable Control of Magnetic Levitation System," *Journal of Robotics and Control*, vol. 4, no. 2, pp. 141-148, 2023, https://doi.org/10.18196/jrc.v4i2.17537.

[18] N. F. Al-Muthairi, M. Zribi, "Sliding mode control of a magnetic levitation system," *Mathematical problem in engineering*, vol. 2004, no. 2, pp. 93-107, 2004, https://doi.org/10.1155/S1024123X04310033.

[19] A. Ma'arif, M. A. M. Vera, M. S. Mahmoud, E. Umoh, A. J. Abougarair, and S. N. Rahmadhia, "Sliding Mode Control Design for Magnetic Levitation System," *Journal of Robotics and Control*, vol. 3, no. 6, pp. 848-853, 2023, https://doi.org/10.18196/jrc.v3i6.12389.

[20] R. Uswarman, S. Istiqphara, and D. H. T. N., "Sliding Mode Control with Gain-Scheduled for Magnetic Levitation System," *Jurnal Ilmiah Teknik Elektro Komputer dan Informatika*, vol. 5, no. 1, pp. 36-43, 2019, https://doi.org/10.26555/jiteki.v5i1.13223.

[21] I. Ahmad and M. A. Javaid, "Nonlinear model & controller design for magnetic levitation system," *Proceedings of the 9th WSEAS international conference on Signal processing, robotics and automation (ISPRA'10)*, pp. 324-328, 2010, https://dl.acm.org/doi/abs/10.5555/1807817.1807874.

[22] S. A. Al-Samarraie, I. I. Gorial and M. H. Mshari, "An integral sliding mode control for the magnetic levitation system based on backstepping approach," *IOP Conference Series: Materials Science and Engineering*, vol. 881, no. 1, p. 012136, 2020, https://doi.org/10.1088/1757-899X/881/1/012136.

[23] Z. N. Mahmood, H. Al-Khazraji and S. M. Mahdi, "PID-based enhanced flower pollination algorithm controller for drilling process in a composite material," *Annales de Chimie - Science des Matériaux*, vol. 47, no. 2, pp. 91-96, 2023, https://doi.org/10.18280/acsm.470205.

[24] R. Al-Majeez, K. Al-Badri, H. Al-Khazraji, and S. M. Ra'afat, "Design of A Backstepping Control and Synergetic Control for An Interconnected Twin-Tanks System: A Comparative Study," *International Journal of Robotics & Control Systems*, vol. 4, no. 4, pp. 2041-2054, 2024, https://doi.org/10.31763/ijrcs.v4i4.1682.

[25] F. R. Yaseen, M. Q. Kadhim, H. Al-Khazraji, and A. J. Humaidi, "Decentralized control design for heating system in multi-zone buildings based on whale optimization algorithm," *Journal Européen des Systèmes Automatisés*, vol. 57, no. 4, pp. 981-989, 2024, https://doi.org/10.18280/jesa.570406.

[26] M. A. AL-Ali, O. F. Lutfy, and H. Al-Khazraji, "Investigation of Optimal Controllers on Dynamics Performance of Nonlinear Active Suspension Systems with Actuator Saturation," *Journal of Robotics and Control (JRC)*, vol. 5, no. 4, pp. 1041-049, 2024, https://doi.org/10.18196/jrc.v5i4.22139.

[27] H. Al-Khazraji, K. Al-Badri, R. Almajeez, and A. J. Humaidi, "Synergetic control-based sea lion optimization approach for position tracking control of ball and beam system," *International Journal of Robotics & Control Systems*, vol. 4, no. 4, pp. 1547-1560, 2024, https://doi.org/10.31763/ijrcs.v4i4.1551.

[28] H. Al-Khazraji, K. Al-Badri, R. Al-Majeez, and A. J. Humaidi, "Synergetic control design based sparrow search optimization for tracking control of driven-pendulum system," *Journal of Robotics and Control (JRC)*, vol. 5, no. 5, pp. 1549-1556, 2024, https://doi.org/10.18196/jrc.v5i5.22893.

[29] R. Al-Majeez, K. Al-Badri, H. Al-Khazraji and S. M. Ra'afat, "Design of A Backstepping Control and Synergetic Control for An Interconnected Twin-Tanks System: A Comparative Study," *International Journal of Robotics and Control Systems*, vol. 4, no. 4, pp. 2041-2054, 2024, https://doi.org/10.31763/ijrcs.v4i4.1682.

[30] H. Al-Khazraji, "Comparative study of whale optimization algorithm and flower pollination algorithm to solve workers assignment problem," *International Journal of Production Management and Engineering*, vol. 10, no. 1, pp. 91-98, 2022, https://doi.org/10.4995/ijpme.2022.16736.

[31] H. Al-Khazraji, S. Khlil, and Z. Alabacy, "Cuckoo search optimization for solving product mix problem," *IOP Conference Series: Materials Science and Engineering*, vol. 1105, no. 1, pp. 1-9, 2021, https://doi.org/10.1088/1757-899X/1105/1/012016.

[32] T. A Nguyen, and T. N. Tran, "Analysis of Swarm Size and Iteration Count in Particle Swarm Optimization for Convolutional Neural Network Hyperparameter Optimization in Short-Term Load Forecasting," *Buletin Ilmiah Sarjana Teknik Elektro*, vol. 7, no. 3, pp. 481-495, 2025, https://doi.org/10.12928/biste.v7i3.13953.

[33] S. Khlil, H. Al-Khazraji, and Z. Alabacy, "Solving assembly production line balancing problem using greedy heuristic method," *IOP Conference Series: Materials Science and Engineering*, vol. 745, no. 1, pp. 1-7, 2020, https://doi.org/10.1088/1757-899X/745/1/012068.

[34] H. Al-Rammahi, and A. Y. Asaad, "A Particle Swarm Optimization-Enhanced Support Vector Regression Model for Accurate Prediction of Concrete Compressive Strength Using Slump Test Data," *Control Systems and Optimization Letters*, vol. 3, no. 3, pp. 272-279, 2025, https://doi.org/10.59247/csol.v3i3.224.

[35] H. Al-Khazraji, S. Khlil, Z. Alabacy, "Industrial picking and packing problem: Logistic management for products expedition," *Journal of Mechanical Engineering Research and Developments*, vol. 43, no. 2, pp. 74-80, 2020, https://www.researchgate.net/publication/339000088.

[36] A. F. A. Ahmed, I. M. Elzein, M. M. Mahmoud, S. A. E. M. Ardjoun, A. M. Ewias, and U. Khaled, "Optimal Controller Design of Crowbar System for DFIG-based WT: Applications of Gravitational Search Algorithm," *Buletin Ilmiah Sarjana Teknik Elektro*, vol. 7, no. 2, pp. 122-137, 2025, https://doi.org/10.12928/biste.v7i2.13027.

[37] H. Al-Khazraji, W. Guo, and A. J. Humaidi, "Improved cuckoo search optimization for production inventory control systems," *Serbian Journal of Electrical Engineering*, vol. 21, no. 2, pp. 187-200, 2024, https://doi.org/10.2298/SJEE2402187A.

[38] L. T. Rasheed, "An optimal modified Elman-PID neural controller design for DC/DC Boost converter model," *Journal of Engineering Science and Technology (JESTEC)*, vol. 18, no. 2, pp. 880-901, 2023, https://jestec.taylors.edu.my/Vol%2018%20Issue%202%20April%202023/18_2_4.pdf.

[39] Z. N. Mahmood, H. Al-Khazraji, and S. M. Mahdi, "Adaptive control and enhanced algorithm for efficient drilling in composite materials," *Journal Européen des Systèmes Automatisés*, vol. 56, no. 3, pp. 507-512, 2023, https://doi.org/10.18280/jesa.560319.

[40] N. Thongpance *et al*., "Comparative analysis of PID tuning methods for speed control in Mecanum-wheel electric wheelchairs," *Buletin Ilmiah Sarjana Teknik Elektro*, vol. 7, no. 2, pp. 95-110, 2025, https://doi.org/10.12928/biste.v7i2.13046.

[41] R. A. Kadhim, M. Q. Kadhim, H. Al-Khazraji, and A. J. Humaidi, "Bee algorithm based control design for two-links robot arm systems," *IIUM Engineering Journal*, vol. 25, no. 2, pp. 367-380, 2024, https://doi.org/10.31436/iiumej.v25i2.3188.

[42] A. K. Ahmed, H. Al-Khazraji, and S. M. Raafat, "Optimized PI-PD control for varying time delay systems based on modified Smith predictor," *International Journal of Intelligent Engineering & Systems*, vol. 17, no. 1, pp. 331-342, 2024, https://doi.org/10.22266/ijies2024.0229.30.

[43] S. D. Perkasa, P. Megantoro, and S. A. Jasmine, "Quantum-Behaved Particle Swarm Optimization-Tuned PI Controller of a SEPIC Converter," *Control Systems and Optimization Letters*, vol. 3, no. 2, pp. 144-150, 2025, https://doi.org/10.59247/csol.v3i2.186.

[44] M. Q. Kadhim, F. R. Yaseen, H. Al-Khazraji and A. J. Humaidi, "Application of Terminal Synergetic Control Based Water Strider Optimizer for Magnetic Bearing Systems," *Journal of Robotics and Control (JRC)*, vol. 5, no. 6, pp. 1973-1979, 2024, https://doi.org/10.18196/jrc.v5i6.23867.

[45] M. Nawfal, A. A. Yahya, R. A. Mahmod, and H. Al-Khazraji, "Integration of Sparrow Search Optimization with Terminal Synergetic Control for Permanent Magnet Linear Synchronous Motors," *Journal of Robotics and Control (JRC)*, vol. 6, no. 2, pp. 1033-1040, 2025, https://doi.org/10.18196/jrc.v6i2.26174.

[46] F. R. Yaseen, and H. Al-Khazraji, "Optimized Vector Control Using Swarm Bipolar Algorithm for Five-Level PWM Inverter-Fed Three-Phase Induction Motor," *International Journal of Robotics & Control Systems*, vol. 5, no. 1, pp. 333-347, 2025, https://doi.org/10.31763/ijrcs.v5i1.1713.

[47] S. Saremi, S. Mirjalili, and A. Lewis, "Grasshopper optimisation algorithm: theory and application," *Advances in Engineering Software*, vol. 105, pp. 30-47, 2017, https://doi.org/10.1016/j.advengsoft.2017.01.004.

[48] Y. Meraihi, A. B. Gabis, S. Mirjalili and A. Ramdane-Cherif, "Grasshopper Optimization Algorithm: Theory, Variants, and Applications," *IEEE Access*, vol. 9, pp. 50001-50024, 2021, https://doi.org/10.1109/ACCESS.2021.3067597.

[49] O. S. Elazab, H. M. Hasanien, I. Alsaidan, A. Y. Abdelaziz, and S. M. Muyeen, "Parameter estimation of three diode photovoltaic model using grasshopper optimization algorithm," *Energies*, vol. 13, no. 2, p. 497, 2020, https://doi.org/10.3390/en13020497.

[50] S. Z. Mirjalili, S. Mirjalili, S. Saremi, H. Faris, and I. Aljarah, "Grasshopper optimization algorithm for multi-objective optimization problems," *Applied Intelligence*, vol. 48, pp. 805-820, 2018, https://doi.org/10.1007/s10489-017-1019-8.

[51] A. A. Ewees, M. A. Gaheen, Z. M. Yaseen and R. M. Ghoniem, "Grasshopper Optimization Algorithm With Crossover Operators for Feature Selection and Solving Engineering Problems," *IEEE Access*, vol. 10, pp. 23304-23320, 2022, https://doi.org/10.1109/ACCESS.2022.3153038.

[52] B. Hekimoğlu and S. Ekinci, "Grasshopper optimization algorithm for automatic voltage regulator system," *2018 5th International Conference on Electrical and Electronic Engineering (ICEEE)*, pp. 152-156, 2018, https://doi.org/10.1109/ICEEE2.2018.8391320.

[53] H. Al-Khazraji, C. Cole, and W. Guo, "Analysing the impact of different classical controller strategies on the dynamics performance of production-inventory systems using state space approach," *Journal of Modelling in Management*, vol. 13, no. 1, pp. 211-235, 2018, https://doi.org/10.1108/JM2-08-2016-0071.

[54] T. Sato, H. Tajika, R. Vilanova, and Y. Konishi, "Adaptive PID control system with assigned robust stability," *IEEJ Transactions on Electrical and Electronic Engineering*, vol. 13, no. 8, pp. 1169-1181, 2018, https://doi.org/10.1002/tee.22680.

[55] R. A. Mahmod, R. A. Kadhima, M. Nawfal, and H. Al-Khazraji, "High Gain Observer Based Backstepping Control Design for Nonlinear Single-Axis Driven Systems," *International Journal of Robotics and Control Systems*, vol. 5, no. 3, pp. 1886-1899, 2025, https://doi.org/10.31763/ijrcs.v5i3.1984.